Quantum molecular dynamics simulations of warm dense lithium hydride: Examination of mixing rules

D. A. Horner, J. D. Kress, and L. A. Collins
Theoretical Division, Los Alamos National Laboratory, Los Alamos, New Mexico 87545, USA
(Received 12 December 2007; published 6 February 2008)

We have performed a systematic study of lithium hydride (LiH) in a density range from half to twice solid for temperatures from 0.5 to 3.0 eV using quantum molecular dynamics (QMD) methods and have tested density and pressure mixing rules for obtaining equations of state and optical properties such as frequency-dependent absorption coefficients and Rosseland mean opacities. The QMD simulations for the full LiH fluid served as a benchmark against which to assess the rules. In general, the mixing rule based on the pressure matching produces superior equations of state and mean opacities for the mixture except at the very lowest temperatures and densities. However, the frequency-dependent absorption coefficients displayed considerable differences in some frequency ranges except at the highest temperatures and densities.

DOI: 10.1103/PhysRevB.77.064102 PACS number(s): 61.20.Ja, 52.25.Os

I. INTRODUCTION

Throughout the universe, matter exits predominately in the form of mixtures from interstellar space to the core of the Earth. In particular, mixtures of hydrogen (H) and helium (He) play an important role in the structure and dynamics of a wide variety of astrophysical objects. For example, the behavior and relative abundances of H/He at high compressions and at temperatures of a few thousand Kelvin control the structure and thermal output of large gas planets such as Jupiter and Saturn.[1] Since most extrasolar planets[2] discovered to date resemble the gas giants, knowledge of the equation of state (EOS) and various dynamical properties of these two species greatly aids in understanding their composition and mass distribution. Such mixtures also exist in the atmospheres of White Dwarfs (WDs).[3] The mixture opacities constitute an important component in determining WD cooling rates, which in turn may serve as an astrochronometer, untainted by cosmological effects. In a more terrestrial vein, the characterization of mixtures under extreme conditions becomes critical to the design of inertial confinement fusion (ICF) capsules and high energy density physics experiments. While the main fuel element in ICF pellets consists of deuterium and tritium (DT), their various layers, composed of beryllium, plastics, and gold, can become highly mixed into the D/T during the implosion.[4] Similarly, the melting and energy-transfer properties of materials[5] during intense laser irradiation can depend on the concentrations of various impurities. All of the above-mentioned physical environments encompass the special regime of warm dense matter (WDM).[6]

While the precise boundaries of this WDM domain remain subject to some debate among the various disciplines, the general range covers temperatures from a few thousand to a few million Kelvin (10^3–10^6 K) and densities from around solid to many times compressed (10^{22}–10^{26} atoms/cm^3). More importantly, the regime can encompass a motley crowd of denizens, consisting of free electrons, molecules, atoms, negative and/or positive ions, and clusters, that continuously interact to change the consistency. WDM environments resemble a highly transitory miasmic brew. The interest in WDM stems not only from important applications but also from the novel processes that arise including phase transitions, transient clustering, and nonequilibrium phenomena.

To model such an environment requires an integrated approach in order to follow the many interaction paths and constituents that arise in this complicated concoction. Electrons behave quantum mechanically, interactions extend across large samples of particles, and transient interchanges occur among the constituents. The development of quantum molecular dynamics (QMD) methods[7–9] has brought considerable progress in the detailed understanding of WDM regimes. By combining a sophisticated quantal treatment of the electrons, usually through a density-functional prescription for a large sample of atoms, with molecular dynamics to effect nuclear motion, QMD permits a consistent determination of static (equation of state), dynamical, and optical properties of complex, extended systems and thus provides a powerful tool for exploring the WDM environs.

For the WDM regime, pure systems have received considerable attention from QMD approaches. A highly select but representative sample includes deuterium as related to recent Hugoniot experiments,[9,10] helium under planetary conditions,[11] aluminum in exploding wires,[12,13] gold under laser irradiation,[14] and hydrogen opacities with astronomical implications.[15] Due to their broad applications, mixtures have begun to garner intense scrutiny with studies, for example, of N-O for shock compression,[16] He-H in regard to planetary interiors and atmospheres,[17] and Au-Al with ICF implications.[18] In addition, some of these studies have employed the properties of the full fluid mixture to validate certain common mixing rules. These mixing rules provide prescriptions for combining data from the individual atomic elements to predict the properties, usually EOS and opacities, of the composite. Since QMD calculations become computationally prohibitive for producing the large data sets employed in macroscopic modeling, mixing rules operating on purely atomic information supplied by simple prescriptions such as the average-atom model[20] must for now suffice. Therefore, determining the validity of these mixing rules from comparisons with sophisticated QMD calculations on

the full mixture becomes imperative to establishing the accuracy of data bases employed in large-scale simulations, for example, radiation hydrodynamics.

In this paper, we contribute to this growing exploration of mixtures in the WDM regime by performing a systematic examination of lithium hydride (LiH) in a density range from half (0.39 g/cm^3) to twice (1.58 g/cm^3) solid for temperatures from 0.5 eV (5800 K) to 3.0 eV (35 000 K) using QMD methods. In addition, we test various mixing rules for obtaining equations of state and optical properties such as frequency-dependent absorption coefficients and Rosseland mean opacities. We combine the results from QMD calculations on pure Li and H samples according to set prescriptions to produce properties of the mixture and employ QMD simulations for the full LiH fluid as a benchmark against which to assess the rules. Subsequent sections of the paper provide a brief theoretical description (Sec. II), followed by a detailed presentation and discussion of the results (Sec. III), and ending with a short conclusion (Sec. IV).

II. FORMALISM

A. Molecular dynamics simulations

We have performed QMD simulations for hydrogen (H), lithium (Li), and lithium hydride (LiH) employing the Vienna *ab initio* simulation package (VASP)[21] within the isokinetic ensemble (constant *NVT*). The electrons received a full quantum mechanical treatment through plane-wave, finite-temperature-density-functional theory (FTDFT) calculations within the Perdew-Wang 91 generalized gradient approximation (GGA) having the ion-electron interaction represented by a projector augmented wave (PAW) pseudopotential.[22] The nuclei evolved classically according to a combined force provided by the ionic repulsion and electronic density. The system was assumed in local thermodynamical equilibrium with the electron (T_e) and ion (T_i) temperatures equal ($T_e = T_i$) in which the former was fixed within the FTDFT and the latter kept constant through simple velocity scaling.

At each time step t for a periodically replicated cell of volume (V) containing N_e active electrons and N_i ions in fixed spatial positions $\mathbf{R}_q(t)$, we first perform a FTDFT calculation within the Kohn-Sham (KS) construction to determine a set of electronic state functions $[\Psi_{i,\mathbf{k}}(t)|i=1,n_b]$ for each k point $\mathbf{k}$,

$$H_{KS}\Psi_{i,\mathbf{k}}(t) = \epsilon_{i,\mathbf{k}}\Psi_{i,\mathbf{k}}(t), \tag{1}$$

with $\epsilon_{i,\mathbf{k}}$, the eigenenergy. The ions are then advanced with a velocity Verlet algorithm, based on the force from the ions and electronic density, to obtain a new set of positions and velocities. Repeating these two steps propagates the system in time yielding a trajectory consisting of the positions and velocities $[\mathbf{R}_q(t),\mathbf{V}_q(t)]$ of the ions and a collection of state functions $[\Psi_{i,\mathbf{k}}(t)]$ for the electrons. These trajectories produce a *consistent* set of static, dynamical, and optical properties.

All simulations employed only Γ point ($\mathbf{k}=0$) sampling of the Brillouin zone and 108 atoms for the pure species (H,Li) and 216 atoms for the mixture (LiH) in a cubic cell of length L ($V=L^3$). We described the hydrogen-electron interaction by a PAW with a maximum energy cutoff (E_{max}) of 400 eV, while, for lithium, we employed a single-electron PAW also with $E_{max}=400$ eV. A sufficient number of bands n_b were included so that the occupation of the highest band was 1×10^{-5} or less. We also tested the sensitivity to the pseudopotentials by using a stiffer hydrogen form with $E_{max}=700$ eV and a three-electron Li form; we found less than a 10% difference in the electronic pressure and optical properties. Trajectories were generally evolved for 1–2 ps with time steps of 0.5 fs for the lower temperatures and 0.25 fs for the higher.

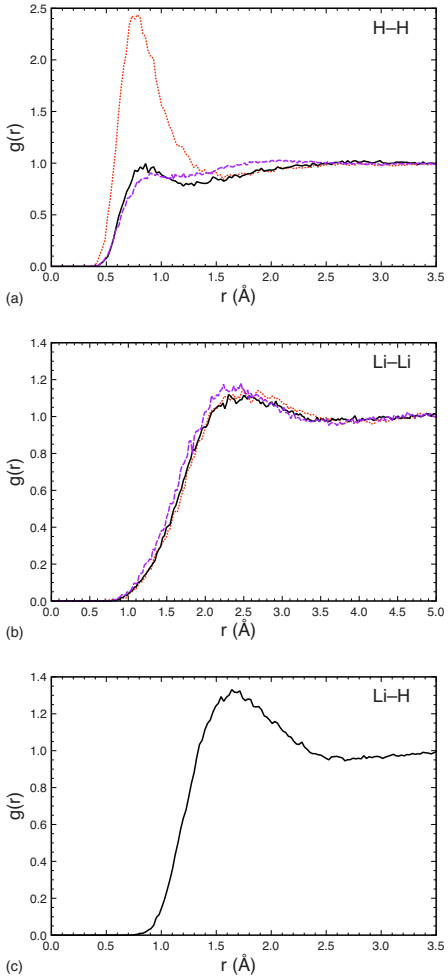

FIG. 1. (Color online) Radial distribution functions: (a) $g_{\text{H-H}}$ (upper panel), (b) $g_{\text{Li-Li}}$ (middle panel), and (c) $g_{\text{Li-H}}$ (lower panel) at 1.0 eV for a mixture density of 0.7874 g/cm^3. In the upper panel, the different curves correspond to a LiH mixture, $V=1824$ Å^3 [black (solid)]; pure H, $V=1824$ Å^3 [red (dot)] MRd; and pure H, $V=424$ Å^3 [violet (dash)] MRp. In the middle panel, the different curves correspond to a LiH mixture, $V=1824$ Å^3 [black (solid)]; pure Li, $V=1824$ Å^3 [red (dot)] MRd; and pure Li, $V=1400$ Å^3 [violet (dash)] MRp. The single curve in the lower panel corresponds to a LiH mixture.

B. Static and Dynamic properties

The total pressure of the system consists of the sum of the electron pressure P_e, computed via the forces from the DFT

TABLE I. Self-diffusion coefficients ($cm^2\ s^{-1}$) as a function of temperature and density. Column labeled H (Li) gives results for a pure hydrogen (lithium) system of 108 atoms in a volume V_{LiH}. The labels H (LiH) and Li (LiH) present the self-diffusion of hydrogen and lithium, respectively, within a LiH mixture of 108 H atoms and 108 Li atoms for V_{LiH}. Volumes 3649, 1824, and 912 $Å^3$, respectively, correspond to densities of the mixture of 0.3937, 0.7874, and 1.575 g/cm^3. Number in brackets indicates power of 10.

T (eV)	V_{LiH} ($Å^3$)	D ($cm^2\ s^{-1}$)			
		H	Li	H (LiH)	Li (LiH)
0.5	3649	1.22[−2]	2.72[−3]	1.03[−2]	2.39[−3]
	1824	9.47[−3]	1.93[−3]	4.27[−3]	1.58[−3]
	912	6.93[−3]	1.20[−3]	1.97[−3]	9.79[−4]
1.0	3649	3.74[−2]	6.63[−3]	2.33[−2]	6.07[−3]
	1824	3.21[−2]	4.39[−3]	1.16[−2]	4.12[−3]
	912	2.46[−2]	3.06[−3]	5.75[−3]	2.73[−3]
2.0	1824	9.98[−2]	1.09[−2]	2.74[−2]	9.20[−3]
	912	7.62[−2]	6.93[−3]	1.35[−2]	5.66[−3]
3.0	1824	1.55[−1]	1.67[−2]	4.37[−2]	1.12[−2]
	912	9.08[−2]	1.24[−2]	2.24[−2]	8.67[−3]

calculation, and the ideal gas pressure of the ions,

$$P = P_e + \frac{nk_BT}{V}. \tag{2}$$

The electronic pressure we report in the tables and text is an average over the pressures at different times along the MD trajectory once the system has equilibrated.

The diffusion coefficient D is computed from the trajectory by either the mean square displacement

$$D = \frac{1}{6t}\langle|\mathbf{R}_i(t) - \mathbf{R}_i(0)|^2\rangle \tag{3}$$

or by the velocity autocorrelation function

$$D = \frac{1}{3}\int_0^\infty \langle\mathbf{V}_i(t)\cdot\mathbf{V}_i(0)\rangle dt. \tag{4}$$

The brackets indicate statistical summations over the trajectories.

From the trajectory, we compute the radial distribution function $g(r)$, which gives the probability of finding two particles at a distance r apart. In the current set of simulations, three radial distributions ($g_{H\text{-}H}$, $g_{Li\text{-}Li}$, and $g_{Li\text{-}H}$) provide valuable information about the arrangement of ions in space.

C. Electrical and optical properties

The real part of the frequency-dependent electrical conductivity provides the basic underlying component for computing a wealth of optical information such as index of refraction, reflectivity, and opacity.[13,15,23–25] The complex electrical conductivity has the form $\sigma(\omega)=\sigma_1(\omega)+i\sigma_2(\omega)$ with the real part given by

$$\sigma_1(\omega) = \frac{2\pi}{\Omega}\sum_{i,j} F_{ij}|D_{ij}|^2\delta(\epsilon_i - \epsilon_j - \omega), \tag{5}$$

where Ω is the atomic volume and ϵ_i is the energy of the ith state. The quantities summed are the difference between the Fermi-Dirac (FD) distributions at temperature T,

$$F_{ij} = [f_{FD}(\epsilon_i) - f_{FD}(\epsilon_j)]/\omega, \tag{6}$$

and the velocity dipole matrix elements computed from the VASP code,

$$|D_{ij}|^2 = \frac{1}{3}\sum_p |\langle\Psi_{i,0}|\nabla_p|\Psi_{j,0}\rangle|^2, \tag{7}$$

with p representing the directions x, y, and z. For practicality, the δ function in Eq. (5) is approximated by a Gaussian as

$$\delta(x) \approx \frac{1}{\sqrt{\pi}\Delta}\exp[-(x/\Delta)^2]. \tag{8}$$

In turn, the imaginary part of the conductivity derives directly from a principle-value (P) integral over the real part,

$$\sigma_2(\omega) = -\frac{2}{\pi}P\int \frac{\sigma_1(\nu)\omega}{(\nu^2-\omega^2)}d\nu. \tag{9}$$

Using the complex conductivity, the components of the dielectric function $\epsilon(\omega)=\epsilon_1(\omega)+i\epsilon_2(\omega)$ are

$$\epsilon_1(\omega) = 1 - \frac{4\pi}{\omega}\sigma_2(\omega), \tag{10}$$

$$\epsilon_2(\omega) = \frac{4\pi}{\omega}\sigma_1(\omega). \tag{11}$$

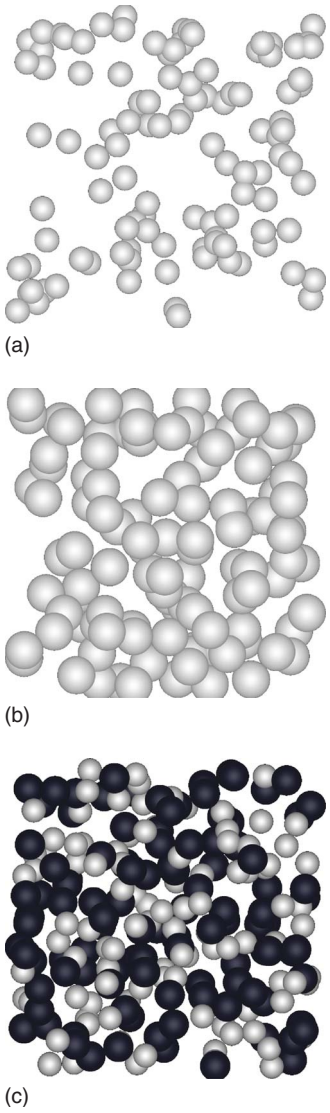

FIG. 2. (Color online) Snapshot of atomic positions for Li (dark gray) and H (light gray) at a temperature of 1.0 eV. Left, pure hydrogen in a volume of 1824 Å^3; center, pure hydrogen in a volume of 424 Å^3; right, LiH mixture in a volume of 1824 Å^3.

Furthermore, the real $n(\omega)$ and imaginary $k(\omega)$ parts of the index of refraction become

$$n(\omega) = \frac{1}{2}\sqrt{|\epsilon(\omega)| + \epsilon_1(\omega)}, \tag{12}$$

$$k(\omega) = \frac{1}{2}\sqrt{|\epsilon(\omega)| - \epsilon_1(\omega)}, \tag{13}$$

and these properties can be further combined to give the reflectivity $r(\omega)$ and the absorption coefficient $\alpha(\omega)$,

$$r(\omega) = \frac{[1-n(\omega)]^2 + k(\omega)^2}{[1+n(\omega)]^2 + k(\omega)^2}, \tag{14}$$

$$\alpha(\omega) = \frac{4\pi}{n(\omega)}\sigma_1(\omega). \tag{15}$$

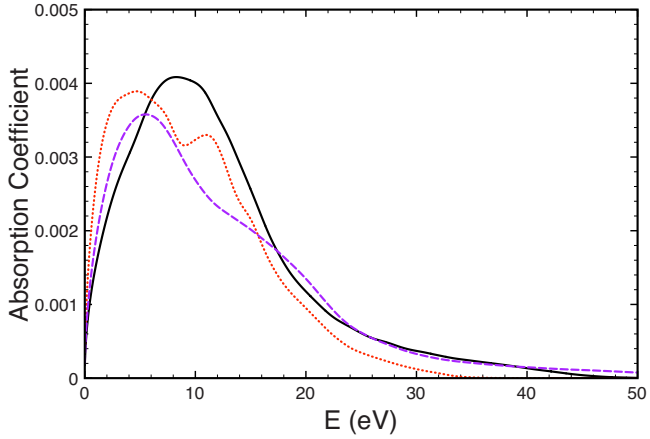

FIG. 3. (Color online) Absorption coefficient for LiH in a volume of 1824 Å^3 and 1.0 eV. Mixture [black (solid)], density matching [red (dot)], and pressure matching [violet (dash)].

Finally, the Rosseland mean opacity (RMO) κ_R is given by

$$\frac{1}{\kappa_R} = \int_0^\infty \frac{B'(\nu)}{\alpha(\nu)} d\nu, \tag{16}$$

where $B'(\nu)$ is the derivative, with respect to temperature, of the normalized Planck function. Since the function $B'(\nu)$ peaks around $4k_BT$, we expect that the computed opacities will be most sensitive to differences in the absorption coefficient around this energy.

The evolution of the MD simulations depends only on the total force on the ions. The FTDFT employs a Fermi-Dirac distribution to populate the eigenstates. Since no contribution to the electronic component of the force arises from unoccupied states, the number of states can be truncated upon reaching a small occupation value. However, given the difference term of FD distributions in Eq. (5), the electrical conductivity depends on excitations between occupied and unoccupied states. Therefore, convergence of the optical properties requires considerably more states than the force. For a representative set of independent snapshots (ionic positions) from a MD trajectory, we recalculate at the Γ point the electronic state function using a large number of bands, typically up to 1000. The electrical conductivity, as well as other optical properties derived from this state function, generally converges for averages over 10–20 snapshots, each separated by the e-folding time for the trajectory. We used a Gaussian broadening Δ of 1 eV in all conductivity calculations. Tests at the Baldereschi point[26] and over four k points show sensitivities in the RMO of less than 5% compared to the Γ point. The large sample sizes (100–200 atoms) employed and the disorder of the liquid account to a great extent for the insensitivity of the optical properties to the number of k points. This choice of parameters produces a consistent set of QMD simulations and properties for the accurate assessment of the various models and rules investigated.

TABLE II. Electronic pressures (GPa) for the mixture and for the density (MRd) and pressure (MRp) mixing rules as a function of temperature and volume. Volumes 3649, 1824, and 912 Å^3, respectively, correspond to densities of the mixture of 0.3937, 0.7874, and 1.575 g/cm^3.

T (eV)	V (Å^3)	P_e (GPa)		
		LiH	MRd	MRp
0.5	3648.7	0.10	−0.65	
	1824.3	13.2	7.4	
	912.1	97.0	54.9	105.9
1.0	3648.7	2.2	0.71	
	1824.3	19.2	12.0	23.2
	912.1	106.7	56.3	111.7
2.0	1824.3	30.6	19.3	32.0
	912.1	127.4	73.8	128.2
3.0	1824.3	43.3	31.3	44.0
	912.1	150.2	94.1	147.9

D. Mixing rules

We examine various mixing rules by which certain properties from pure species are combined by some prescription to determine the properties of the mixture, for example, pressure and opacities. The *standard* of comparison consists of a full QMD calculation of the LiH mixture for a sample of 216 atoms of equal numbers of hydrogen (N_H=108) and lithium (N_{Li}=108) in a volume V_{LiH} at a given temperature T (=T_e), which produces a pressure P_{LiH} and optical properties $[\alpha_{LiH}, \kappa_{LiH}]$. Such a simulation includes all interactions among the atoms in the cell and their periodic images and can represent such transient features as molecular bonding, ionization, and recombination. At this temperature, we also perform two QMD simulations for the pure systems of hydrogen and lithium, each with 108 atoms and volumes of V_H and V_{Li}, respectively, and obtain individual pressures $[P_H, P_{Li}]$ and absorption coefficients $[\alpha_H, \alpha_{Li}]$. We consider two representative mixing rules:[18,19] density matching (MRd) and pressure matching (MRp).

In the density matching (MRd), we have set the volume of the individual species to that of the total mixture $[V_H = V_{Li} = V_{LiH}]$ and performed QMD simulations for H at a density of N_H/V_{LiH} and Li at N_{Li}/V_{LiH}. We then determine a total pressure (absorption) by simply adding the individual pressures (absorption coefficients) from the separate H and Li QMD simulations. The density matching rule (MRd) consists of the following prescription:

$$V_{LiH} = V_H = V_{Li}, \tag{17}$$

$$P^d{}_{LiH} = P_H + P_{Li}, \tag{18}$$

$$\alpha^d{}_{LiH} = \alpha_H + \alpha_{Li}. \tag{19}$$

We have added a superscript to designate properties derived from a particular mixing rule, as opposed to those for the full mixture. For the pressure, the density mixing rule basically follows an ideal gas prescription for noninteracting Li and H gases in a volume V_{LiH}.

The pressure matching rule (MRp) involves a more complicated construction. In this case, we must perform a series of QMD simulations on the individual species in which the volumes are varied under the constraint $[V^p{}_{LiH} = V_H + V_{Li}]$ until the individual pressures agree $[P_H = P_{Li}]$. The total pressure becomes P_H (or equally P_{Li}), and the absorption coefficients are combined by volume fractions. The MRp then consists of the following prescription:

$$V_{LiH} = V_H + V_{Li}, \tag{20}$$

$$P^p{}_{LiH} = P_H = P_{Li}, \tag{21}$$

$$\alpha^p{}_{LiH} = \left(\frac{V_H}{V_{LiH}}\right)\alpha_H + \left(\frac{V_{Li}}{V_{LiH}}\right)\alpha_{Li}. \tag{22}$$

For both mixing cases, the Rosseland mean opacity is then found by integrating the combined absorption coefficients, as indicated in Eq. (16).

We should emphasize that the comparison of the above mixing rules represents a "best case scenario" since the properties of the individual species themselves originate from QMD calculations. While divorced of the Li-H interactions, these pure-species simulations still encompass complex intra-atomic interactions over large samples of atoms. In many mixture studies, the properties of pure species derive from perturbed-atom models, which treat a single representative atom within a cell whose boundary conditions are ad-

TABLE III. Rosseland mean opacities (cm^{-1}) for the mixture and for the density (MRd) and pressure (MDp) mixing rules as a function of temperature and volume. Volumes 3649, 1824, and 912 Å^3, respectively, correspond to densities of the mixture of 0.3937, 0.7874, and 1.575 g/cm^3. Number in brackets indicates power of 10.

T (eV)	V (Å^3)	κ_R (cm^{-1})		
		LiH	MRd	MRp
0.5	3649	2.89[+5]	3.22[+5]	
	1824	3.57[+5]	5.55[+5]	
	912	4.50[+5]	7.26[+5]	6.82[+5]
1.0	1824	5.58[+5]	6.85[+5]	6.59[+5]
	912	7.49[+5]	1.10[+6]	8.31[+5]
2.0	1824	5.61[+5]	5.18[+5]	5.40[+5]
	912	9.74[+5]	1.11[+6]	1.05[+6]
3.0	1824	3.10[+5]	2.43[+5]	3.30[+5]
	912	7.68[+5]	6.19[+5]	7.58[+5]

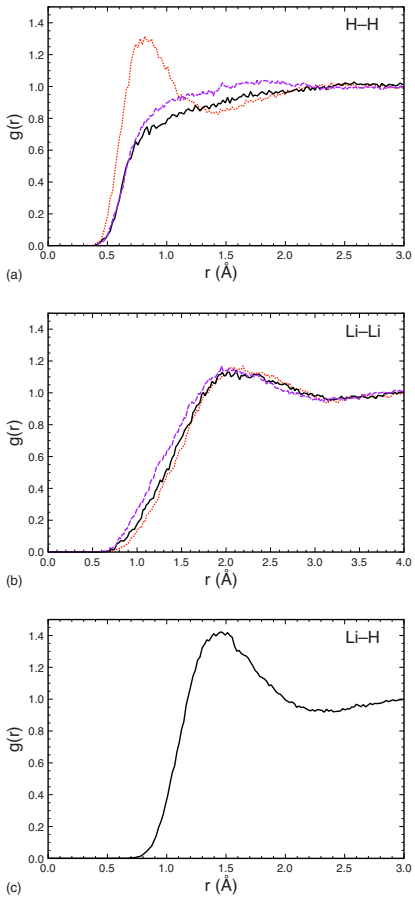

FIG. 4. (Color online) Radial distribution functions: (a) $g_{\text{H-H}}$ (upper panel), (b) $g_{\text{Li-Li}}$ (middle panel), and (c) $g_{\text{Li-H}}$ (lower panel) at 1.0 eV for a mixture density of 1.575 g/cm^3. In the upper panel, the different curves correspond to a LiH mixture, V=912 Å^3 [black (solid)]; pure H, V=912 Å^3 [red (dot)] MRd; and pure H, V =254 Å^3 [violet (dash)] MRp. In the middle panel, the different curves correspond to a LiH mixture, V=912 Å^3 [black (solid)]; pure Li, V=912 Å^3 [red (dot)] MRd; and pure Li, V=658 Å^3 [violet (dash)] MRp. The single curve in the lower panel corresponds to a LiH mixture.

justed to introduce effects from the surrounding medium. These "average-atom" models[20] approximate to some extent the environments of the fluid state experienced by the pure species in the QMD simulations.

E. Results and discussion

As an initial test of our techniques, we compared to the results of Ogitsu *et al.*,[27] who performed similar calculations on LiH at lower temperatures but comparable densities. While their simulations employed constant pressure constraints, we could find conditions for which our *NVT* calculations gave similar properties. For example, at a density of 28.5 a_B^3/atom and a temperature of 3000 K, we obtained a pressure of 86 GPa in good agreement with their value of 100 GPa. We found that the diffusion coefficients agreed in this case as well as the structure in the pair correlation functions, including the small H_2 molecular component. These

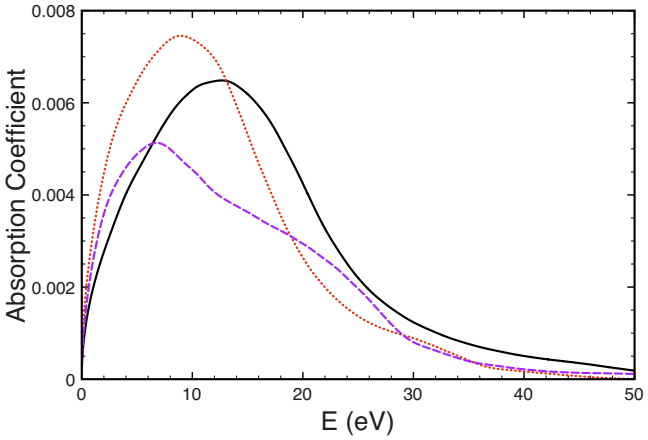

FIG. 5. (Color online) Absorption coefficient for LiH in a volume of 912 Å^3 and 1.0 eV. Mixture [black (solid)], density matching [red (dot)], and pressure matching [violet (dash)].

comparisons provide validation for our procedures and choice of parameters.

We determine the validity of the mixing rules over a range of temperatures from 0.5 eV (5.6×10^3 K) to 3.0 eV (3.5×10^4 K) and densities from half (0.3937 g/cm^3) to twice (1.5749 g/cm^3) solid for LiH. We generally report the density in terms of the mixture volume V_{LiH} in Å^3 for N_{LiH} =216 atoms (0.7874 g/cm^3 ≡ 1824.3 Å^3). For these conditions, the LiH system forms a *fluid*. This becomes apparent from the linear slope attained by the mean square displacement at longer times, permitting the extraction of self-diffusion coefficients by Eq. (3). In Table I, we present the self-diffusion coefficients for the pure hydrogen and lithium fluids as well as the lithium hydride mixture. The results for the pure species correspond to two noninteracting ideal gases of Li and H within a volume V_{LiH}. While the Li diffusion within the mixture does not deviate more than 30% from the pure result, the behavior of the H shows considerable sensitivity to its environment, varying by as much as a factor of 4. This indicates qualitatively that interactions with the Li may play an important role in the motion of hydrogen within the mixture.

Tables II and III summarize the general trends in the electronic pressure and RMOs, while Table IV gives partial volumes and densities for the MRp case. In the case of the pressure, the mixing rules generally bracket the results for the full mixture with the pressure prescription (MRp) generally producing better results across the entire temperature and density range. For example, at the lowest temperature (0.5 eV) and highest density (1.58 g/cm^3), the pressure from the MRd lies about 43% lower than the mixture, while the MRp gives a value 9% higher. As the temperature rises at this density, the electronic pressure for the MRd remains about 37%–47% below the mixture. On the other hand, by 1.0 eV, the MRp pressure reaches to within 5% of the mixture and retains this accuracy for higher temperatures. The situation for the Rosseland mean opacities appears even better with both mixing rules performing well for temperatures above 0.5 eV. Global properties can, in some situations, be misleading as to the degree to which a prescription accu-

TABLE IV. Volumes (Å^3) for 108 atoms and densities (g/cm^3) used for the MRp simulations.

T (eV)	V_{LiH}	ρ_{LiH}	V_{H}	ρ_{H}	V_{Li}	ρ_{Li}
0.5	912	1.58	250	0.71	662	1.90
1.0	1824	0.79	424	0.42	1400	0.90
	912	1.58	254	0.70	658	1.91
2.0	1824	0.79	450	0.40	1374	0.92
	912	1.58	262	0.68	650	1.93
3.0	1824	0.79	464	0.39	1360	0.92
	912	1.58	256	0.70	656	1.92

rately reproduces the actual nature of the fully mixed system. To this end, we examine several representative cases in greater detail. The RMO, in particular, samples only a very narrow photon-energy (frequency) range due to the sharp peak in the Planck function around $4k_B$T. Since, for example, radiation transport applications now require absorption characteristics over a considerable span in photon energy, we must determine the broader validity of these mixing rules for optical properties. In addition, other applications require a deeper understanding of the detailed structure of the media, as characterized by the pair correlation functions.

We first consider the composite fluid at 1.0 eV at the density of solid LiH (0.78 g/cm^3 V_{LiH}=1824 Å^3 N_{LiH}=216 atoms). For this case, the pressure matching yields a volume for H of 424 Å^3, significantly less than the mixture, and for Li of 1400 Å^3. The MRd and MRp give electronic pressures (opacities) within 38% (23%) and 21% (18%) of the mixture, respectively. Figure 1 displays the pair correlation functions for the mixture and mixing rules. The upper panel shows distinct differences for $g_{\mathrm{H\text{-}H}}$. The density mixing produces a H sample with a considerable concentration of diatomic molecules, as indicated by the strong peak around 0.746 Å, the equilibrium internuclear distance R_{eq} for H_2, in constrast to the separation in the solid structure of 2.8 Å. However, both the mixture and the MRp produce only a very weak molecular signature. This depletion of H_2 occurs for the pure H sample due to the high density required by the MRp and for the mixture due to the presence of the Li. On the other hand, as indicated by the middle panel, which displays $g_{\mathrm{Li\text{-}Li}}$, all models yield about the same general distribution of lithium and show no characteristic molecular component. This result does not appear surprising given that Li has roughly the same density in each case. Finally, the lower panel presents $g_{\mathrm{Li\text{-}H}}$ for the mixture, which has a broad peak in the vicinity of the equilibrium separation for the LiH molecule (R_{eq} =1.60 Å). This feature can only occur for the mixture and indicates an important component missing from the mixing-rule formulations.

We gain further insight into the nature of the pure and mixed fluids by examining actual snapshots of the atom positions, as depicted in Fig. 2. To keep the same perspective, we have made the box sizes the same and increased the relative size of the atoms in the case of the smaller volume. The right-hand panel displays the full complexity of the mixture with the H and Li intricately intertwined. On the other hand, the pure hydrogen in the mixture volume (1824 Å^3) has considerable open spaces as well as molecules. When the volume of the pure H is reduced as in the MRp case (424 Å^3, center panel), the unoccupied space greatly diminishes. A certain concern arises—even though certain properties derived from the mixing rules may agree with the results of the full mixture, their internal details may still contain considerable deficiencies.

In Fig. 3, we carry the comparison further by examining the absorption coefficients. Even though the RMOs agree to with in 20%, the behavior with photon energy evinces considerable differences. The α_{LiH} peaks around 10 eV, while those from the mixing rules show maxima closer to 5 eV. The MRd even has a double-peak structure not evident in the mixture. Care must thus be exercised in employing the frequency-dependent absorption coefficients from mixing rules over an extended energy range.

We continue our study by treating the same temperature (1.0 eV) at an increased density of the mixture to twice that of the solid (1.58 g/cm^3 V_{LiH}=912 Å^3 N_{LiH}=216 atoms). The MRp gives volumes of 254 Å^3 for H and 658 Å^3 for Li, producing significantly better results for electronic pressure (opacity) when compared to the mixture and yielding percentage differences of 5% (11%) as opposed to 47% (47%) for the MRd. Figure 4 gives the verdict on the structure of the resulting fluids. Once again, the Li distributions appear in good agreement for all three cases, as indicated by the middle panel. The MRd still has a distinct H_2 peak although reduced by a factor of 2 from lower densities, while the mixture and the MRp have very similar H distributions. At this density, we cannot make a firm identification of a LiH molecular feature from the $g_{\mathrm{Li\text{-}H}}$ function since the R_{eq} of the molecule and the nearest-neighbor distance in the solid crystal are about the same. Still, a correlation in the Li and H positions persists. Figure 5 shows that differences remain in the absorption coefficients over the frequency range. The peak of the MRd has moved closer to that of the mixture even though the Rosseland has become less accurate; rather large disagreements survive in the α coefficients for MRp and the mixture. While an increase in density has improved the agreement, especially for the pressure rule, distinct and important differences remain in the optical details.

The final example involves raising the temperature to 2.0 eV for the denser case (1.58 g/cm^3). For the MRp, we

obtain volumes of 262 and 650 Å^3 for pure H and Li, respectively, which change little from the 1.0 eV result. The electronic pressures (opacities) differ from the mixture by 42% (14%) for MRd and 1% (8%) for MRp. The general structure of the fluids again comes from the behavior of the pair correlation functions, as given in Fig. 6. The distributions for the H-H and Li-Li have similar behavior. In contrast with the previous two cases, the molecular hydrogen peak has disappeared for the MRd. The general structure now resembles a fully atomic fluid. Similarly for the absorption, we discern a considerably closer alignment in the shapes and magnitudes of the MRp and the mixture (Fig. 7).

The generation of the pressure matching results required us to explore the EOS of the pure species. For hydrogen, the regime encompassed the realm transversed by the principal Hugoniot that starts from the cryogenic liquid. The FTDFT-GGA gives good agreement with certain experiments as well as with quantum path integral Monte Carlo simulations and

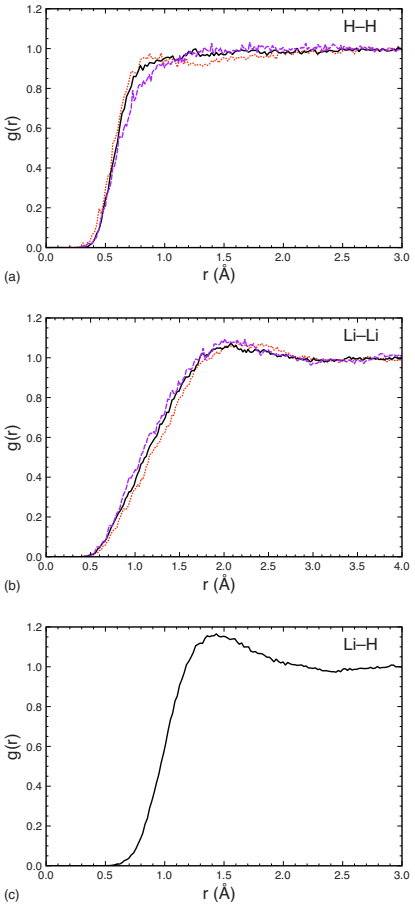

FIG. 6. (Color online) Radial distribution functions: (a) $g_{\text{H-H}}$ (upper panel), (b) $g_{\text{Li-Li}}$ (middle panel), and (c) $g_{\text{Li-H}}$ (lower panel) at 2.0 eV for a mixture density of 1.575 g/cm^3. In the upper panel, the different curves correspond to a LiH mixture, V=912 Å^3 [black (solid)]; pure H, V=912 Å^3 [red (dot)] MRd; and pure H, V=262 Å^3 [violet (dash)] MRp. In the middle panel, the different curves correspond to a LiH mixture, V=912 Å^3 [black (solid)]; pure Li, V=912 Å^3 [red (dot)] MRd; and pure Li, V=650 Å^3 [violet (dash)] MRp. The single curve in the lower panel corresponds to a LiH mixture.

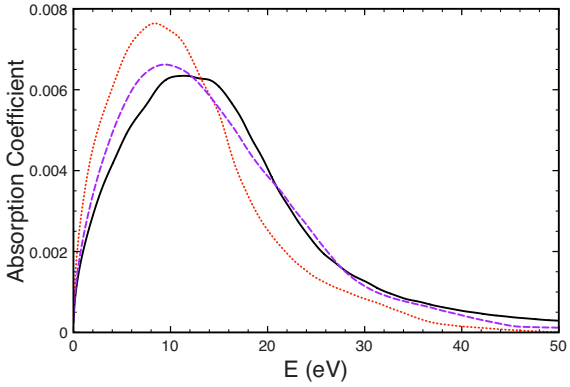

FIG. 7. (Color online) Absorption coefficient for LiH in a volume of 912 Å^3 and 2.0 eV. Mixture [black (solid)], density matching [red (dot)], and pressure matching [violet (dash)].

the chemical model, as represented in the SESAME library. A detailed comparison appears elsewhere.[9,10] Experimental results for Li are lacking for the regime covered by this study. However, we obtained structure factors and diffusion coefficients within or very near the experimental error bars for solid density and low temperatures (470–800 K) and in close accord with other QMD calculations.[28]

III. CONCLUSIONS

We have performed a systematic study of lithium hydride (LiH) in a density range from half (0.39 g/cm^3) to twice (1.58 g/cm^3) solid for temperatures from 0.5 eV (5800 K) to 3.0 eV (35 000 K) using QMD methods and have tested density and pressure mixing rules for obtaining equations of state and optical properties such as frequency-dependent absorption coefficients and Rosseland mean opacities. Combining the results from QMD calculations on pure Li and H samples according to set prescriptions produced properties of the mixture. The QMD simulations for the full LiH fluid served as a benchmark against which to assess the rules. In general, the mixing rule based on the pressure matching produced superior pressures and mean opacities for mixtures. However, the frequency-dependent absorption coefficients displayed considerable differences in some frequency ranges except at the highest temperatures and densities.

ACKNOWLEDGMENTS

We acknowledge useful discussions with and suggestions by F. Lambert, J. Clerouin, S. Mazevet, and G. Zerah of Commissariat à l'Energie Atomique, Bruyére-le-Châtel, France, on the implementation and character of the mixing rules. This work has been supported by the Advanced Scientific Computing Program. The Los Alamos National Laboratory is operated by Los Alamos National Security, LLC for the National Nuclear Security Administration of the U.S. Department of Energy under Contract No. DE-AC52-06NA25396.

[1] T. Guillot, D. J. Stevenson, W. B. Hubbard, and D. Saumon, in *Jupiter*, edited by F. Bagenal (University of Arizona Press, Tucson, 2003), Chap. 3, pp. 35–57.
[2] N. C. Santos, W. Benz, and M. Mayor, Science **310**, 251 (2005); A. Burrows, Nature (London) **433**, 261 (2005).
[3] G. Fountaine, P. Brassard, and P. Bergeron, Publ. Astron. Soc. Pac. **113**, 409 (2001).
[4] J. Paiser, J. Boyes, S. Kumpman, W. Lowdermilk, and M. Soren, Laser Focus World **30**, 75 (1994).
[5] K. Widmann, T. Ao, M. Foord, D. Price, A. Ellis, P. Springer, and A. Ng, Phys. Rev. Lett. **92**, 125002 (2004).
[6] L. Collins, J. Kress, and S. Mazevet, Los Alamos Sci. **29**, 70 (2005).
[7] L. Collins, I. Kwon, J. Kress, N. Troullier, and D. Lynch, Phys. Rev. E **52**, 6202 (1995); L. Collins, J. Kress, T. Lenosky, N. Troullier, and I. Kwon, J. Comput.-Aided Mater. Des. **5**, 173 (1998).
[8] D. Hohl, V. Natoli, D. M. Ceperley, and R. M. Martin, Phys. Rev. Lett. **71**, 541 (1993); J. I. Penman, J. G. Clerouin, and P. G. Zerah, Phys. Rev. E **51**, R5224 (1995); J. Kohanoff and J.-P. Hansen, Phys. Rev. E **54**, 768 (1996); O. Pfaffenzeller and D. Hohl, J. Phys.: Condens. Matter **9**, 11 023 (1997); S. Bagnier, P. Blottiau, and J. Clerouin, Phys. Rev. E **63**, 015301 (2000).
[9] G. Galli, R. Q. Hood, A. U. Hazi, and F. Gygi, Phys. Rev. B **61**, 909 (2000).
[10] T. J. Lenosky, S. R. Bickham, J. D. Kress, and L. A. Collins, Phys. Rev. B **61**, 1 (2000); M. P. Desjarlais, *ibid.* **68**, 064204 (2003).
[11] B. Militzer, Phys. Rev. Lett. **97**, 175501 (2006); A. Kietzmann, B. Holst, R. Redmer, M. Desjarlais, and T. Mattson, *ibid.* **98**, 190602 (2007); S. Mazevet, M. Challacombe, P. Kowalski, and D. Saumon, Astrophys. Space Sci. **307**, 273 (2007).
[12] S. Mazevet, M. P. Desjarlais, L. A. Collins, J. D. Kress, and N. H. Magee, Phys. Rev. E **71**, 016409 (2005).
[13] M. P. Desjarlais, J. D. Kress, and L. A. Collins, Phys. Rev. E **66**, 025401(R) (2002).
[14] S. Mazevet, J. Clerouin, V. Recoules, P. M. Anglade, and G. Zerah, Phys. Rev. Lett. **95**, 085002 (2005).
[15] S. Mazevet, L. Collins, N. Magee, J. Kress, and J. Keady, Astron. Astrophys. **405**, L5 (2003).
[16] S. Mazevet, P. Blottiau, J. D. Kress, and L. A. Collins, Phys. Rev. B **69**, 224207 (2004).
[17] J. Vorberger, I. Tamblyn, B. Miltzer, and S. A. Bonev, Phys. Rev. B **75**, 024206 (2007).
[18] J. Clerouin, V. Recoules, S. Mazevet, P. Noiret, and P. Renaudin, Phys. Rev. B **76**, 064204 (2007).
[19] F. Lambert, J. Clerouin, J.-F. Danel, L. Kazanfjian, and G. Zerah, Phys. Rev. E (to be published).
[20] R. M. More, Adv. At. Mol. Phys. **21**, 305 (1985); W. Johnson, C. Guet, and G. Bertsch, J. Quant. Spectrosc. Radiat. Transf. **99**, 327 (2006).
[21] G. Kresse and J. Hafner, Phys. Rev. B **47**, RC558 (1993); G. Kresse and J. Furthmüller, Comput. Mater. Sci. **6**, 15 (1996); G. Kresse and J. Furthmüller, Phys. Rev. B **54**, 11169 (1996).
[22] G. Kresse and D. Joubert, Phys. Rev. B **59**, 1758 (1999); P. E. Blöchl, *ibid.* **50**, 17953 (1994).
[23] J. Callaway, *Quantum Theory of the Solid State* (Academic, New York, 1974).
[24] W. A. Harrison, *Solid State Theory* (Mc Graw-Hill, New York, 1970).
[25] L. A. Collins, S. R. Bickham, J. D. Kress, S. Mazevet, T. J. Lenosky, N. J. Troullier, and W. Windl, Phys. Rev. B **63**, 184110 (2001).
[26] A. Baldereschi, Phys. Rev. B **7**, 5212 (1973).
[27] T. Ogitsu, E. Schwegler, F. Gygi, and G. Galli, Phys. Rev. Lett. **91**, 175502 (2003).
[28] S. Wang, S. J. Mitchell, and P. A. Rikvold, Comput. Mater. Sci. **29**, 145 (2004) and references therein; J. Anta and P. Madden, J. Phys.: Condens. Matter **11**, 6099 (1999); G. Kresse, J. Non-Cryst. Solids **205**, 833 (1996).